ROYAL SOCIETY OPEN SCIENCE

royalsocietypublishing.org/journal/rsos

Research

Cite this article: Qu X, Bian Y, Li J, Pan Y, Bai Y. 2019 A red fluorescent BODIPY probe for iridium (III) ion and its application in living cells. *R. Soc. open sci.* **6**: 181090.
http://dx.doi.org/10.1098/rsos.181090

Received: 10 July 2018
Accepted: 11 December 2018

Subject Category:
Biochemistry and biophysics

Subject Areas:
biochemistry

Keywords:
BODIPY probe, iridium (III) ion probe, fluorescence imaging

Author for correspondence:
Yongjun Bian
e-mail: yjbian2013@jzxy.edu.cn

Electronic supplementary material is available online at https://dx.doi.org/10.6084/m9.figshare.c.4358516.

THE ROYAL SOCIETY PUBLISHING

A red fluorescent BODIPY probe for iridium (III) ion and its application in living cells

Xingyu Qu, Yongjun Bian, Jianqing Li, Yufeng Pan and Yang Bai

Department of Chemistry and Chemical Engineering, Jinzhong University, Jinzhong, Shanxi 030619, China

XQ, 0000-0003-1081-3462

A new red fluorescent probe **1** based on BODIPY skeleton has been successfully synthesized through introduction of 2-(thiophen-2-yl) quinoline moiety at *meso*- and 3-position, which exhibits excellent optical performance, including high fluorescence quantum yield, large pseudo Stokes' shift as well as high selectivity and sensitivity towards iridium (III) ion in aqueous solution and in living cells.

1. Introduction

Fluorescence imaging microscopy is an essential and potent tool for monitoring the analytes inside living systems based on sensitive optical response of probes to the analytes [1–5]. A fluorescence signal is characterized by its intensity, wavelength, lifetime and polarization. In fluorescence imaging, intensity used to create images can reflect the localization and concentration of the probe [6–10]. Many fluorescence probes have been synthesized to increase photo-stability and tune the emission into red or near-infrared region (NIR) (600–900 nm) to avoid photobleaching of emissive dyes and deepen penetration depths during fluorescence imaging [11–17]. BODIPY dyes show the highest potential due to many excellent features, such as the relatively high molar absorption coefficients and fluorescence quantum yields, narrow emission bandwidths with high peak intensities, the robustness against light and chemicals and accessibility of versatile dyes [18–22]. The red or NIR BODIPY probe can be easily obtained, by the introduction of aromatic or heteroaromatic rings as substituents at the 3, 5 and/or 1, 7 positions on the pyrrole moieties [23–25]. The widely used mechanisms for BODIPY probes are photoinduced electron transfer (PET), photoinduced intramolecular charge transfer (ICT) and resonance energy transfer (RET). Many BODIPY probes based on PET are often built as fluorophore–spacer–chelator constructs, in which appending the chelator at the *meso*-position of the BODIPY

fluorophore decouples the two subunits [26–29]. Whereas, many BODIPY probes based on ICT often introduced the chelator in the 3, 5 and/or 1, 7 positions on the pyrrole moieties making ratiometric measurements possible [30–33].

Iridium is a rare but very useful metal that can be used in many fields including catalytic converters, luminescent materials, anti-cancer drugs, electrodes, fuel cells and jewellery etc. [34–38]. Especially in organic chemistry, like other heavy-metal catalysts such as palladium and platinum, iridium compounds as the catalysts could also effectively promote the transformation between various functional groups [39,40]. However, the wide use of these heavy-metals has resulted in an increase of residue levels into environment, especially ambient air and soil, which is harmful to public health. As some research findings showed, the iridium exposure could affect an immune imbalance and cause contact urticaria with anaphylactic reactions [41,42]. Thus, the oral permissible daily exposure (PDE) for iridium impurity is less than 100 μg per day by US Pharmacopeia [43]. Therefore, the recognition and detection of these heavy-metal ions have been a considerably significant and active research area. Numerous methods, particularly fluorescent methods, have been developed for the detection of palladium and platinum [44–53]. Among those, Kaur *et al.* reported the 'off-on' type fluorescence probe based on the BODIPY core for Pd^{2+} detection [49]. To the best of our knowledge, only an example was reported for Ir^{3+} detection to date [54]. Accordingly, exploring highly selective and sensitive probes for Ir^{3+} detection is very necessary due to the potential hazards to human health. In our previous work, we reported a BODIPY probe with a 2-(thiophen-2-yl)quinoline group as a chelator can selectively and sensitively detect the Fe^{3+} ion [55,56]. Herein, we report that functionalization of the pyrrole moieties of BODIPY with 2-(thiophen-2-yl)quinoline (TQ) tunes the dye for Ir^{3+} detection. Furthermore, fluorescence microscopy experiments demonstrated that resulting probe **1** could be used to monitor Ir^{3+} ion in living cells.

2. Material and methods

2.1. Reagents and instruments

Unless otherwise noted, the reagents or solvents were obtained from commercial suppliers and used without further purification. Metal salts, such as $IrCl_3 \cdot 3H_2O$, $RhCl_3 \cdot 3H_2O$, $AuCl_3$, $AgNO_3$, $PdCl_2$, $PtCl_2$, $FeCl_3 \cdot 6H_2O$, $AlCl_3$, $Cd(NO_3)_2 \cdot 4H_2O$, $CrCl_3$, $CuCl_2 \cdot 2H_2O$, $Hg(OAc)_2$, $Ni(OAc)_2 \cdot 4H_2O$, $Pb(OAc)_2 \cdot 3H_2O$, $Zn(OAc)_2 \cdot 2H_2O$, $Co(OAc)_2 \cdot 4H_2O$, were used for making metal solutions. All air and moisture sensitive reactions were carried out under an argon atmosphere. Dry CH_2Cl_2 was obtained by refluxing and distilling over CaH_2 under nitrogen. Triethylamine was obtained by simple distillation.

The ^1H NMR and ^{13}C NMR spectroscopic measurements were made by using a Bruker AVF-400 or a Bruker 700 MHz spectrometer. The measurements for ^1H NMR and ^1H-^1H COSY were performed at 700 MHz (DRX-700) or 400 MHz (DRX-400). The measurements for ^{13}C NMR were performed at 175 MHz (DRX-700). Mass spectra were measured with a Bruker ultraflex MALDI TOF MS spectrometer and Thermo Scientific LTQ Orbitrap XL spectrometer. Fluorescence spectral measurements were carried out by using a Hitachi F-4600 fluorescence spectrophotometer. Electronic absorption spectra were recorded with Shimadzu UV-2550 spectrophotometers.

2.2. Synthetic procedures for probe **1**

The synthesis of probe **1** is outlined in scheme 1. The compounds **2** and **3** were produced according to a published procedure [55]. Probe **1** was prepared through Knoevenagel condensation of compound **2** and 5-(Quinolin-2-yl)thiophene-2-carbaldehyde **3** according to the below procedure and characterized by MALDI-TOF MS, HR-MS, ^1H NMR, ^{13}CNMR.

2.3. Procedures for metal ion sensing

Stock solutions of various metal ions (0.1 M), such as Ir^{3+}, Rh^{3+}, Au^{3+}, Fe^{3+}, Al^{3+}, Cd^{2+}, Cr^{3+}, Cu^{2+}, Hg^{2+}, Ni^{2+}, Pb^{2+}, Zn^{2+}, Co^{2+}, Ag^{+}, were prepared in deionized water. Palladium (II) solution (0.1 M) and platinum (II) solution (0.01 M) were prepared in dilute hydrochloric acid. For titration, probe **1** (3 ml, 10 μM, dimethyl sulfoxide solution) was added to the quartz optical cell of 1 cm optical path length. The metal solution was gradually added to probe **1** using a micro-pipette. For selectivity

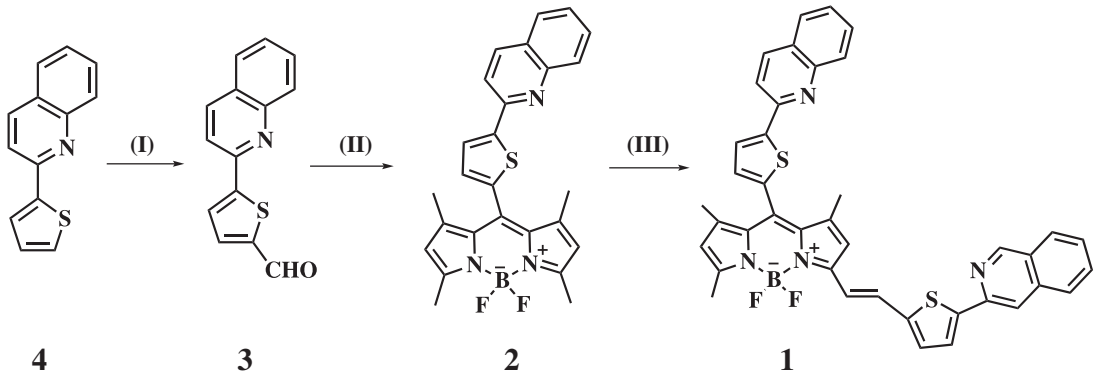

Scheme 1. Synthetic procedures for the preparation of probe **1**. (I) *n*-butlithium and DMF in THF, −78°C (II) 2,4-dimethyl-pyrrole and trifluoroacetic acid in CH_2Cl_2, DDQ, triethylamine, $BF_3 \cdot OEt_2$; (III) 5-(Quinolin-2-yl) thiophene-2-carbaldehyde, AcOH/piperidine, benzene, reflux.

evaluation, the test samples were prepared by adding appropriate amounts of metal ion stock solution to probe **1** (3 ml, 10 μM, dimethyl sulfoxide solution). Fluorescence was measured for 590 nm excitation within 595–800 nm.

2.4. Cell culture and fluorescence bioimaging

The Hela cell line was provided by the Institute of Biochemistry and Cell Biology, SIBS, CAS (China). Cells were grown in high glucose Dulbecco's Modified Eagle Medium (DMEM, 4.5 g of glucose l^{-1}) supplemented with 10% fetal bovine serum (FBS) at 37°C and 5% CO_2. Cells ($5 \times 10^8 l^{-1}$) were plated on 14 mm glass coverslips and allowed to adhere for 24 h. Experiments to assess Ir^{3+} uptake were performed over 1 h in the same medium supplemented with 100 μM $IrCl_3 \cdot 3H_2O$.

Immediately before the experiments, cells were washed with PBS buffer and then incubated with 5 μM probe **1** in PBS buffer for 30 min at 37°C. Cell imaging was then carried out after washing the cells with PBS buffer. Confocal fluorescence imaging was performed with a Zeiss LSM 710 laser scanning microscope and a 63× oil-immersion objective lens. Cells incubated with probe **1** were excited at 590 nm using a multi-line argon laser.

2.5. Theoretical calculations

Geometry optimization and TD-DFT calculations were carried out for probe **1** and probe **1** with Ir^{3+} using the B3LYP functional of the Spartan 16 software packages with 6-31G(d) basis sets.

3. Results and discussion

3.1. Characterization of the probe **1**

Figure 1 shows the UV/visible absorption and emission spectra of compounds **1** and **2** in CH_2Cl_2. The absorption maximum of compound **2** is centred at approximately 514 nm. By contrast, the absorption maxima of probe **1** is red shifted to 625 nm mainly due to the introduction of a TQ substituent at 3-position on the pyrrole moiety. Exciting the 2-(thiophen-2-yl)quinoline moiety at 334 nm in compound **4** provides an emission band at 386 nm. Whereas the emission from the TQ moiety in probe **1** is almost quenched completely upon excitation at 334 nm, strong emissions typical for the BODIPY fluorescence at 635 nm for probe **1** are observed. The fluorescence quantum yield of probe **1** in dimethyl sulfoxide (DMSO) is 0.34 and the pseudo Stokes' shift is up to 300 nm. These results indicate that probe **1** has a large pseudo Stokes' shift and efficient through-bond energy transfer from the TQ donor to the BODIPY acceptor.

3.2. Fluorescence detection and selectivity of probe **1**

The response of probe **1** with Ir^{3+} is investigated by spectrophotometric titration in DMSO, as shown in figure 2. After adding Ir^{3+} from 0 to 100 eq ([metal]/[probe **1**]), the fluorescence intensity of probe **1** at

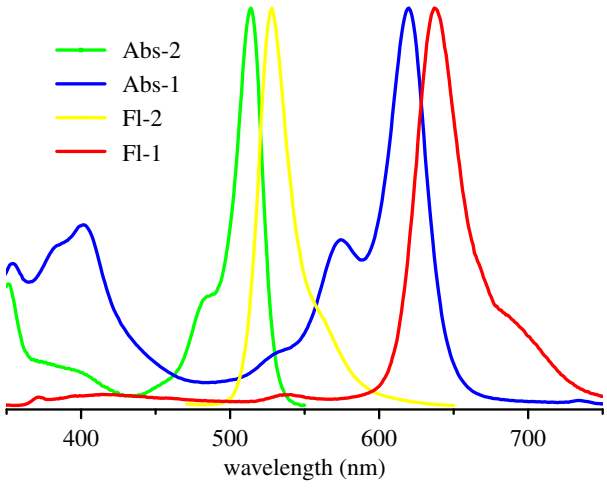

Figure 1. UV–Vis absorption and fluorescence spectra of probe **1** (10 μM) (red line) and compound **2** (10 μM) (green line) in dichloromethane.

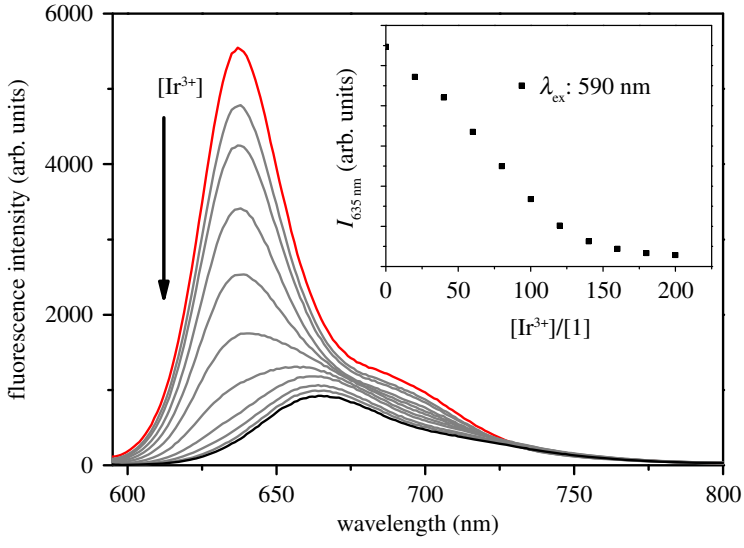

Figure 2. The fluorescence spectrum of probe **1** is (10 μM in DMSO) in the presence of different Ir^{3+} concentration. (Inset) The emission intensity at 635 nm of probe **1** changes as a function of the Ir^{3+} concentration.

635 nm decreased remarkably with a virtually unchanged peak position. Upon addition of more than 100 equiv. of Ir^{3+}, the red shift in the fluorescence peak of probe **1** about 30 nm can be observed. As shown in electronic supplementary material, figure S9, the fluorescence response of probe **1** towards Ir^{3+} is normalized as $R = 1 - I_i/I_{max}$, where I_{max} is fluorescence response of probe **1** without Ir^{3+}, I_i is luminescent intensity of probe **1** with Ir^{3+} [47]. The detection limit of probe **1** for Ir^{3+} is determined as 2.55 ppm based on the signal-to-noise ratio of three. The good linear relationship between the fluorescence response and concentration of Ir^{3+} is obtained with a 0.9910 correlation coefficient.

To gauge the recognition specificity of probe **1** to Ir^{3+} ion, the spectral response features of probe **1** to various interference metal ions with much higher concentration were estimated. The selectivity of probe **1** with Ir^{3+} is examined according to its bonds with various metal ions as shown in figure 3. When the metal ions ([metal]/[probe **1**] = 200:1), such as Fe^{3+}, Al^{3+}, Cd^{2+}, Ag^{+}, Cr^{3+}, Cu^{2+}, Hg^{2+}, Ni^{2+}, Pb^{2+}, Zn^{2+}, are added to the probe **1** solution (10 μM in DMSO), the fluorescence spectrum peak and intensity is nearly unchanged. After the addition of the metal ions (Co^{2+}, Rh^{3+}, Pd^{2+}, Au^{3+}, Pt^{2+}, Ir^{3+}) under the same conditions, the fluorescence intensity decreased by 20%, 20%, 20%, 16%, 33%, 94%, respectively. The above results demonstrate that its Ir^{3+} response is not interfered in the background containing appropriate metal ions.

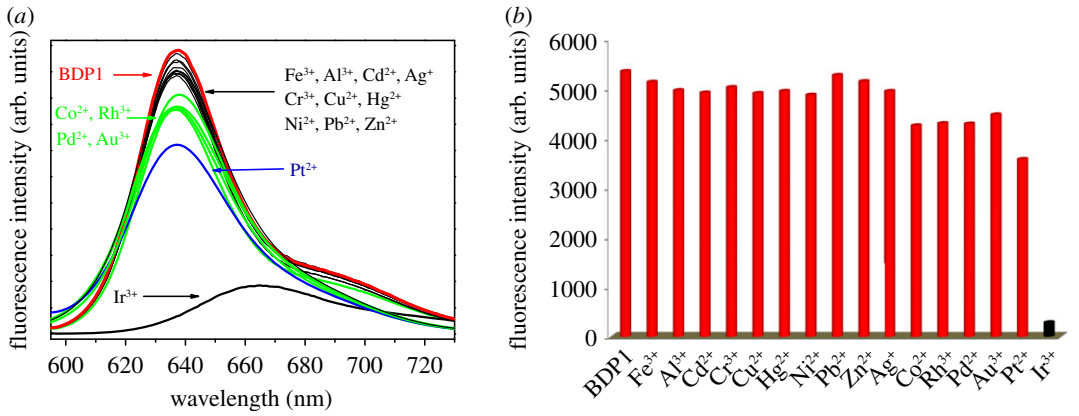

Figure 3. (*a*) Fluorescence spectra of 10 μM probe **1** upon addition of different metal ions in DMSO solution. (*b*) The fluorescence intensity of probe **1** is observed at 635 nm upon addition of various anions.

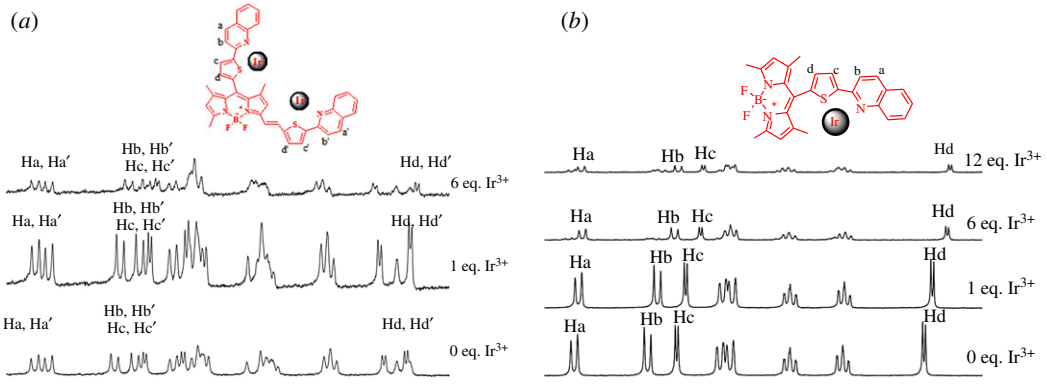

Figure 4. ^{1}H NMR of probe **1** (*a*) and compound **2** (*b*) with different concentrations of Ir^{3+} in DMSO-d_6.

3.3. Sensing mechanism of probe 1 with Ir^{3+}

That probe **1** could selectively monitor Ir^{3+} ion was possible because of the stable binding with sulfur and nitrogen atom in TQ parts. To further demonstrate this mechanism, the binding mode of Ir^{3+} ion with probe **1** or compound **2** is investigated by ^{1}H NMR spectroscopy as shown in figure 4 and electronic supplementary material, figure S7. The ^{1}H NMR spectra of probe **1** and compound **2** in the presence of different concentrations of Ir^{3+} are recorded in DMSO-d_6 and compared to the spectrum of the ion-free probe. During ^{1}H NMR spectra of compound **2**, the protons (Hc and Hd) of the thiophene group at 8.14 ppm and 7.32 ppm are affected significantly by Ir^{3+}. Upon the addition of Ir^{3+}, significant downfield shifts of protons ($\Delta_{Hc} = 0.08$ ppm) and ($\Delta_{Hd} = 0.07$ ppm) corresponding to the protons of the thiophene group are observed, indicating that Ir^{3+} coordinates to the sulfur atom of compound **2**. Furthermore, the proton (Hb) of the quinoline group at 8.24 ppm exhibits a downfield shift ($\Delta_{Hb} = 0.09$ ppm), indicating that Ir^{3+} coordinates to the nitrogen atom of compound **2**. The results indicate that the sulfur atom and nitrogen atom of compound **2** may be involved in coordination to Ir^{3+}. Figure 4 shows that the protons (Hc, Hb, Hd and Hc′, Hb′, Hd′) of probe **1** have significant downfield shifts as well, which indicate that probe **1** and compound **2** have similarities to binding of Ir^{3+} ion.

Probe **1** based on oxidative PET is in the fluorescence 'on' state when in the ion-free form. Coordination of TQ moiety at *meso*-position of probe **1** with Ir^{3+} ion makes it electron poor and lowers the LUMO of TQ moiety. Our theoretical calculation revealed that the LUMO orbital energy of probe **1** with Ir^{3+} is lower, compared to the probe **1**(−2.68 eV versus −4.01 eV) (electronic supplementary material, figure S8), so that PET from the excited BODIPY moiety to the TQ moiety at *meso*-position becomes possible, leading to fluorescence quenching. Probe **1** possesses an electron-donating group (TQ moiety at 3-position) conjugated to an electron-withdrawing group (BODIPY moiety); it undergoes ICT from the donor to the acceptor upon photo-excitation. The interaction of

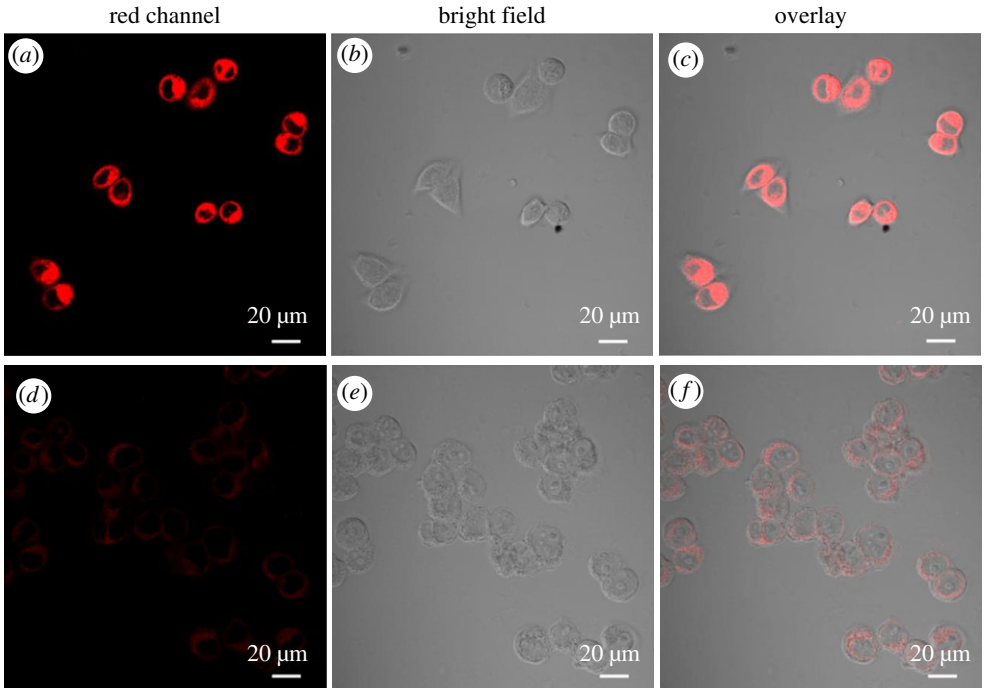

Figure 5. Confocal fluorescence, bright field images and overlay image of probe **1** in Hela cells. (*a*) Cells incubated with 5 μM of probe **1** for 30 min at 37°C upon excitation at 590 nm. (*d*) Cells supplemented with 100 μM of Ir^{3+} in the growth media for 1 h at 37°C upon excitation at 590 nm. (*b,e*) Bright field image of cells shown in panel. (*d,f*) Overlay image of cells shown in panel.

Ir^{3+} ion with the TQ moiety at 3-position enhances the electron-withdrawing character and consequently red shifted the fluorescence spectra.

3.4. Practical application of probe **1**

The practical application of probe **1** as Ir^{3+} probe in living cells has been evaluated. As shown in figure 5, after incubating the Hela cells with 5 μM probe **1** for 30 min at 37°C, a significant green emission from the intracellular region could be observed upon excitation at 590 nm (figure 5*a*). Supplementing cells with 100 μM Ir^{3+} in the growth medium for 1 h at 37°C, microscope images showed only weak intracellular fluorescence (figure 5*d*). Both bright field and overlay measurements with Ir^{3+} and probe **1** after treatment confirmed that the cells are viable throughout the imaging experiments (figure 5*b,c,e,f*). In addition, large signal ratios ($I2/I1 > 20$) are observed at the cytoplasm (region 2) and the nucleus (region 1) due to weak nuclear uptake of probe **1** (electronic supplementary material, figure S10). These data lead to exclusive staining in the cytoplasm, which indicates that probe **1** is cell-permeable. These results indicate that probe **1** can be used as an effective intracellular Ir^{3+} imaging agent.

The cell viability of probe **1** is evaluated through an MTT assay (figure 6). Cell viability is monitored for 5 and 10 h after treatment with probe **1** over a wide range of concentrations (0–80 μM). This demonstrates that probe **1** does not negatively affect the cell viability over the range of concentrations studied, therefore, can clearly be used for the intracellular detection of the Ir^{3+} ion.

4. Conclusion

In summary, we have designed a red BODIPY probe with 2-(thiophen-2-yl)quinoline substituent at *meso*- and 3-position, which exhibits excellent optical performance with a pseudo Stokes' shift (300 nm) and strong emission. The high selectivity and sensitivity of probe **1** towards Ir^{3+} indicate that probe **1** can be used as a fluorescence turn-off sensor for Ir^{3+} in living cells. Probe **1** in fluorescence imaging can avoid photobleaching of emissive dyes and deepen penetration depths. This study displays an effective rationale to design chemosensors for rapid Ir^{3+} sensing in biological systems. Meanwhile, there is still considerable scope for further research in this area for the detection of biologically noble metals.

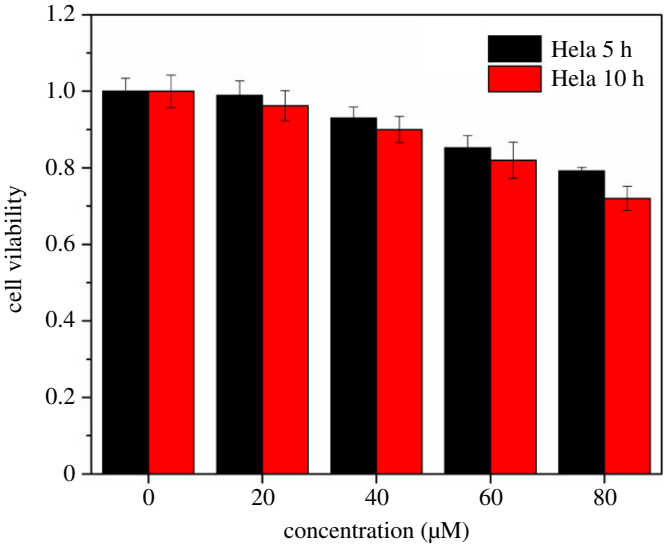

Figure 6. MTT assay of probe **1**.

5. Experimental

5.1. General procedure for synthesis of compound **2**

Compound **2** is synthesized according to the published procedures [55]. Red solid; 65% yield. ^{1}H NMR(DMSO-d_6, 400 MHz): 8.48 (d, 1H, $J = 8$ Hz), 8.24 (d, 1H, $J = 8$ Hz), 8.14 (d, 1H, $J = 4$ Hz), 8.00 (q, 2H, $J = 8$ Hz), 7.77 (t, 1H, $J = 12$ Hz), 7.59 (t, 1H, $J = 12$ Hz), 7.33 (d, 1H, $J = 4$ Hz), 6.26 (s, 2H), 2.47 (s, 6H), 1.72 (s, 6H).

5.2. General procedure for synthesis of probe **1**

Compound **2** (0.22 mmol, 100 mg) and compound **3** (0.26 mmol, 63 mg) are added to a 50 ml round-bottomed flask containing 20 ml benzene solution under an argon atmosphere. And then piperidine (0.4 ml) and acetic acid (0.4 ml) are added to this solution using a syringe. The mixture is heated under reflux by using a Dean Stark trap and reaction was monitored by TLC method. After the starting compound **2** disappearing, the mixture is cooled to room temperature. Then the reaction mixture is washed with water, dried over Na_2SO_4, and concentrated at reduced pressure. The crude product is purified by silica-gel column chromatography using CH_2Cl_2 as the eluent to afford the black power **1**. Yield: 5.5%. ^{1}H NMR($CDCl_3$, 700 MHz): 8.20 (d, 1H, $J = 7$ Hz), 8.16 (d, 1H, $J = 14$ Hz), 8.12 (d, 1H, $J = 7$ Hz), 8.09 (d, 1H, $J = 7$ Hz), 7.85 (d, 1H, $J = 7$ Hz), 7.81–7.78 (m, 5H), 7.72 (t, 1H, $J =$ 7 Hz), 7.68 (s, 1H), 7.62 (d, 1H, $J = 21$ Hz), 7.51 (m, 2H), 7.39 (d, 1H, $J = 14$ Hz), 7.07 (s, 1H), 6.65 (s, 1H), 6.07 (s, 1H), 2.64 (s, 3H), 1.81 (s, 3H), 1.78 (s, 3H). ^{13}C NMR($CDCl_3$, 175 MHz): 156.61, 152.23, 151.76, 151.59, 146.21, 148.04, 147.63, 146.49, 144.92, 143.34, 142.47, 137.80, 136.88, 136.60, 133.88, 132.93, 131.85, 130.14, 130.03, 129.42, 129.34, 129.29, 129.15, 129.09, 127.56, 127.52, 127.38, 127.32, 126.75, 126.53, 126.34, 125.81, 121.88, 119.33, 118.12, 117.59, 117.23, 29.75, 14.24, 14.13. MALDI-TOF MS, calcd. for $C_{40}H_{29}BF_2N_4S_2$: 678.18948; found: 678.208 [M^+]. HR-MS, calcd. for $C_{40}H_{29}BF_2N_4S_2$: 678.18948; found: 678.18976 [M^+].

Data accessibility. The spectroscopic data are submitted to journal as supporting files. The supplementary data are available at http://dx.doi.org/10.6084/m9.figshare.6795095.

Authors' contributions. Y.Bi. conceived, designed and coordinated the study; X.Q. participated in the design, carried out the laboratory work and performed statistical analysis; Y.P. analysed the data; J.L. and Y.Ba. revised the manuscript. X.Q. and Y.Bi. gave final approval for publication.

Competing interests. We declare we have no competing interests.

Funding. This work was supported by Scientific and Technological Innovation Programs of Higher Education Institutions in Shanxi (no. 2015176), the Doctoral Scientific Research Foundation of Jinzhong University (no. bsjj2015213 and no. bsjj2015214), Construction plan of '1331 engineering' photoelectric material innovation team of Jinzhong University and the Fund for Shanxi '1331 Project' Key Innovative Research Team.

Acknowledgements. Authors are most grateful to the professor Z. Shen at Nanjing University, Nanjing, China and professor K.-S. Chan, the Chinese University of Hong Kong, Hong Kong, China.

References

1. Zhang KY, Yu Q, Wei H, Liu S, Zhao Q, Huang W. 2018 Long-lived emissive probes for time-resolved photoluminescence bioimaging and biosensing. *Chem. Rev.* **118**, 1770–1839. (doi:10.1021/acs.chemrev.7b00425)
2. Gao M, Yu F, Lv C, Choo J, Chen L. 2017 Fluorescent chemical probes for accurate tumor diagnosis and targeting therapy. *Chem. Soc. Rev.* **46**, 2237–2271. (doi:10.1039/C6CS00908E)
3. Dolan C, Byrne A, Long C, Czamara K, Kaczor A, Baranska M, Keyes TE. 2017 Polypyridyl substituted BODIPY derivatives; water switchable imaging probes that exhibit halogen substituent dependent localisation in live cells. *RSC Adv.* **7**, 43 743–43 754. (doi:10.1039/C7RA07493J)
4. Yan Y, Tian JW, Hu FR, Wang X, Shen Z. 2016 A near IR photosensitizer based on self-assembled CdSe quantum dot-aza-BODIPY conjugate coated with poly(ethylene glycol) and folic acid for concurrent fluorescence imaging and photodynamic therapy. *RSC Adv.* **6**, 113 991–113 996. (doi:10.1039/C6RA23113F)
5. Zhou J, Gai L, Mack J, Zhou Z, Qiu H, Chan KS, Shen Z. 2016 Synthesis and photophysical properties of orthogonal rhodium(III)-carbon bonded porphyrin-aza-BODIPY conjugates. *J. Mater. Chem. C* **4**, 8422–8428. (doi:10.1039/C6TC03130G)
6. Mahmood Z, Zhao J. 2016 The unquenched triplet excited state of the fluorescent OFF/ON Bodipy-derived molecular probe based on photo-induced electron transfer. *Photochem. Photobiol. Sci.* **15**, 1358–1365. (doi:10.1039/C6PP00307A)
7. Chauhan P, Yan N. 2016 Novel bodipy-cellulose nanohybrids for the production of singlet oxygen. *RSC Adv.* **6**, 32 070–32 073. (doi:10.1039/C6RA04275A)
8. Wang Y, Pan FC, Zhang YL, Peng FF, Huang ZT, Zhang WJ, Zhao WL. 2016 A dual-mode turn-on fluorescent BODIPY-based probe for visualization of mercury ions in living cells. *Analyst* **141**, 4789–4795. (doi:10.1039/C6AN00371K)
9. Guliyev R, Ozturk S, Sahin E, Akkaya EU. 2012 Expanded bodipy dyes: anion sensing using a bodipy analog with an additional difluoroboron bridge. *Org. Lett.* **14**, 1528–1531. (doi:10.1021/ol300260q)
10. Ye Z, Duan C, Hu Q, Zhang Y, Qin C, Zeng L. 2017 A dual-channel responsive near-infrared fluorescent probe for multicolour imaging of cysteine in living cells. *J. Mater. Chem. B* **5**, 3600–3606. (doi:10.1039/C7TB00489C)
11. Zhu H, Cheng P, Chen P, Pu K. 2018 Recent progress in the development of near-infrared organic photothermal and photodynamic nanotherapeutics. *Biomater. Sci.* **6**, 746–765. (doi:10.1039/C7BM01210A)
12. Kowada T, Maeda H, Kikuchi K. 2015 BODIPY-based probes for the fluorescence imaging of biomolecules in living cells. *Chem. Soc. Rev.* **44**, 4953–4972. (doi:10.1039/c5cs00030k)
13. Bi J *et al.* 2017 Near-infrared fluorescent probe for sensitive detection of Pb(II) ions in living cells. *Inorganica Chim. Acta* **468**, 140–145. (doi:10.1016/j.ica.2017.06.044)
14. Zhang S *et al.* 2016 Near-infrared fluorescent probes with large Stokes shifts for sensing Zn(II) ions in living cells. *ACS Sens.* **1**, 1408–1415. (doi:10.1021/acssensors.6b00490)
15. Xia S, Shen J, Wang J, Wang H, Fang M, Zhou H, Tanasova M. 2018 Ratiometric fluorescent and colorimetric BODIPY-based sensor for zinc ions in solution and living cells. *Sens. Actuators B Chem.* **258**, 1279–1286. (doi:10.1016/j.snb.2017.11.129)
16. Wang J, Long L, Xia L, Fang F. 2017 A NIR fluorescent probe for rapid detection of Hg^{2+} in living cells and *in vivo* mice imaging. *Methods Appl. Fluoresc.* **5**, 025002. (doi:10.1088/2050-6120/aa6d8d)
17. Ozdemir T, Sozmen F. 2016 BODIPY based self-healing fluorescent gel formation *via* acylhydrazone linkage. *RSC Adv.* **6**, 10 601–10 605. (doi:10.1039/C5RA22993F)
18. Xu YF, Chang D, Feng S, Zhang C, Jiang JX. 2016 BODIPY-containing porous organic polymers for gas adsorption. *New J. Chem.* **40**, 9415–9423. (doi:10.1039/C6NJ01812B)
19. Aurore L, Kevin B. 2007 BODIPY dyes and their derivatives: syntheses and spectroscopic properties. *Chem. Rev.* **107**, 4891–4932. (doi:10.1021/cr078381n)
20. Goswami PP, Syed A, Beck CL, Albright TR, Mahoney KM, Unash R, Smith EA, Winter AH. 2015 BODIPY-derived photoremovable protecting groups unmasked with green light. *J. Am. Chem. Soc.* **137**, 3783–3786. (doi:10.1021/jacs.5b01297)
21. Ke XS, Kim T, Lynch VM, Kim D, Sessler JL. 2017 Flattened calixarene-like cyclic BODIPY array: a new photosynthetic antenna model. *J. Am. Chem. Soc.* **139**, 13 950–13 956. (doi:10.1021/jacs.7b08611)
22. Lincoln R, Greene LE, Zhang WZ, Louisia S, Cosa G. 2017 Mitochondria alkylation and cellular trafficking mapped with a lipophilic BODIPY–acrolein fluorogenic probe. *J. Am. Chem. Soc.* **139**, 16 273–16 281. (doi:10.1021/jacs.7b08615)
23. Boens N, Leen V, Dehaen W. 2012 Fluorescent indicators based on BODIP. *Chem. Soc. Rev.* **41**, 1130–1172. (doi:10.1039/C1CS15132K)
24. Kaur B, Kaur N, Kumar S. 2018 Colorimetric metal ion sensors—a comprehensive review of the years 2011–2016. *Coord. Chem. Rev.* **358**, 13–69. (doi:10.1016/j.ccr.2017.12.002)
25. Lu H, Mack J, Nyokong T, Kobayashi N, Shen Z. 2016 Optically active BODIPYs. *Coord. Chem. Rev.* **318**, 1–15. (doi:10.1016/j.ccr.2016.03.015)
26. Yang LJ, Liao DJ, Wu AT, Yan HB. 2017 Synthesis and fluorescent properties of aza-crown ether tethered BODIPY fluorophores. *Tetrahedron Lett.* **58**, 889–891. (doi:10.1016/j.tetlet.2017.01.058)
27. Tamada M, Iino T, Wang YM, Ide M. 2017 Facile synthesis of dimeric aza-BODIPY analogues from electron-deficient bislactams and their intriguing optical and electrochemical properties. *Tetrahedron Lett.* **58**, 3151–3154. (doi:10.1016/j.tetlet.2017.06.088)
28. Yan ZX, Lin XR, Guo HY, Yang FF. 2017 A novel fluorescence sensor for K^+ based on bis-Bodipy: the ACQ effect controlled by cation complexation of pseudo crown ether ring. *Tetrahedron Lett.* **58**, 3064–3068. (doi:10.1016/j.tetlet.2017.06.065)
29. Wu XY, Wu WT, Cui XN, Zhao JZ, Wu MB. 2016 Preparation of Bodipy-ferrocene dyads and modulation of the singlet/triplet excited state of bodipy *via* electron transfer and triplet energy transfer. *J. Mater. Chem. C* **4**, 2843–3853. (doi:10.1039/C5TC01222H)
30. Ooyama Y, Hato M, Enoki T, Aoyama S, Furue K, Tsunojia N, Ohshita J. 2016 A BODIPY sensor for water based on a photo-induced electron transfer method with fluorescence enhancement and attenuation systems. *New J. Chem.* **40**, 7278–7281. (doi:10.1039/C6NJ01467D)
31. Nastasi F, Puntoriero F, Serroni S, Campagna S, Olivier JH, Ziessel R. 2014 Photophysical properties of an unusual bichromophoric species constructed from a cyclometalated Pt(II) chromophore and a blue Bodipy-acetylacetonate species. *Dalton Trans.* **43**, 17 647–17 658. (doi:10.1039/C4DT01127A)
32. Nigam S *et al.* 2016 Structurally optimised BODIPY derivatives for imaging of mitochondrial dysfunction in cancer and heart cells. *Chem. Commun.* **52**, 7114–7117. (doi:10.1039/C5CC08325G)
33. Ozdemir T, Bila JL, Sozmen F, Yildirim LT, Akkaya EU. 2016 Orthogonal bodipy trimers as photosensitizers for photodynamic action. *Org. Lett.* **18**, 4821–4823. (doi:10.1021/acs.orglett.6b02418)
34. Kuwabara J, Namekawa T, Sakabe E, Haga M, Kanbara T. 2017 Luminescent Ir(III) complexes bearing benzothiazole or benzoxazole-based pincer ligand. *J. Organomet. Chem.* **845**, 189–195. (doi:10.1016/j.jorganchem.2017.04.037)
35. Xiong K, Chen Y, Ouyang C, Guan RL, Ji LN, Chao H. 2016 Cyclometalated iridium(III) complexes as mitochondria-targeted anticancer agents. *Biochimie* **125**, 186–194. (doi:10.1016/j.biochi.2016.03.013)
36. Mou ZD, Deng N, Zhang F, Zhang JY, Cen J, Zhang X. 2017 'Half-sandwich' Schiff-base Ir(III) complexes as anticancer agents. *Eur. J. Med. Chem.* **138**, 72–82. (doi:10.1016/j.ejmech.2017.06.027)
37. Schlicht S, Haschke S, Mikhailovskii V, Manshina A, Bachmann J. 2018 Highly reversible water

oxidation at ordered nanoporous iridium electrodes based on an original atomic layer deposition. *ChemElectroChem* **5**, 1259–1264. (doi:10.1002/celc.201800152)

38. Cui XH, Fan YB, Hall MB, Burgess K. 2005 Mechanistic insights into iridium-catalyzed asymmetric hydrogenation of dienes. *Chem. Eur. J.* **11**, 6859–6868. (doi:10.1002/chem.200500762)
39. Qu JP, Helmchen G, 2017 Applications of iridium-catalyzed asymmetric allylic substitution reactions in target-oriented synthesis. *Acc. Chem. Res.* **50**, 2539–2555. (doi:10.1021/acs.accounts.7b00300)
40. Iglesias M, Oro LA. 2018 A leap forward in iridium–NHC catalysis: new horizons and mechanistic insights. *Chem. Soc. Rev.* **47**, 2772–2808. (doi:10.1039/C7CS00743D)
41. Bergman A, Svedberg U, Nilsson E. 1995 Contact urticaria with anaphylactic reactions caused by occupational exposure to iridium salt. *Contact Dermatitis* **32**, 14–17. (doi:10.1111/j.16000536.1995.tb00833.x)
42. Iavicoli I, Fontana L, Marinaccio A, Bergamaschi A, Calabrese EJ. 2010 Iridium alters immune balance between t helper 1 and t helper 2 responses. *Hum. Exp. Toxicol.* **29**, 213–219. (doi:10.1177/0960327109360215)
43. United States Pharmacopeia (USP). 2017 USP Elemental Impurities-Limits, US Pharmacopeia – National Formulary, USP 40/NF 35. Rockville, MD: United States Pharmacopeia Convention Inc.
44. Tan H, Liu J, Zhou L, Li Y, Yan J, Zhang L. 2017 A smart NIR fluorescent probe for the highly selective detection of palladium. *RSC Adv.* **7**, 6583–6586. (doi:10.1039/c6ra27502h)
45. Jie X, Liu M, Peng A, Huang J, Zhang Y, Wang X, Tian Z. 2018 A new colorimetric, near-infrared fluorescent probe for rapid detection of palladium with high sensitivity and selectivity. *Talanta* **183**, 164–171. (doi:10.1016/j.talanta.2018.02.019)
46. Xia Q, Feng S, Liu D, Feng G. 2018 A highly selective and sensitive colorimetric and near-infrared fluorescent turn-on probe for rapid detection of palladium in drugs and living cells. *Sens. Actuators B Chem.* **258**, 98–104. (doi:10.1016/j.snb.2017.11.099)
47. Mironenko AY, Tutov MV, Sergeev AA, Bratskaya SY. 2017 On/off rhodamine based fluorescent probe for detection of Au and Pd in aqueous solutions. *Sens. Actuators B Chem.* **246**, 389–394. (doi:10.1016/j.snb.2017.02.092)
48. Shen C, Harris BDW, Dawson LJ, Charles KA, Hambley TW, New EJ. 2015 Fluorescent sensing of monofunctional platinum species. *Chem. Commun.* **51**, 6312–6314. (doi:10.1039/c4cc08077g)
49. Kaur P, Kaur N, Kaur M, Dhuna V, Singh J, Singh K. 2014 'Turn-on' coordination based detection of Pd^{2+} and bioimaging applications. *RSC Adv.* **4**, 16 104–16 108. (doi:10.1039/C3RA47785A)
50. Kuhana AT, Feng WY, Feng GQ. 2018 A simple but effective colorimetric and far-red to near-infrared fluorescent probe for palladium and its application in living cells. *Dyes Pigm.* **152**, 112–117. (doi:10.1016/j.dyepig.2018.01.044)
51. Wen J, Lv YH, Xia PY, Liu FY, Li YQ, Chen SS, Sun SG. 2018 A water-soluble near-infrared fluorescent probe for specific Pd^{2+} detection. *Bioorg. Med. Chem.* **26**, 931–937. (doi:10.1016/j.bmc.2017.12.003)
52. Zhou JL, Xu S, Dong XC, Chen ZJ, Zhao WL. 2018 Near-infrared off-on fluorescent probe for fast and selective detection of palladium (II) in living cells. *J. Photochem. Photobiol. A Chem.* **355**, 158–164. (doi:10.1016/j.jphotochem.2017.09.058)
53. Zhou L, Feng Y, Chen JH, Sun N, Zhou XG, Xiang HF. 2012 Simple, selective, and sensitive colorimetric and ratiometric fluorescence/phosphorescence probes for platinum(II) based on Salen-type Schiff bases. *RSC Adv.* **2**, 10 529–10 536. (doi:10.1039/C2RA21254D)
54. Chen HL, Bao XF, Li F, Zhou B, Ye R, Zhu J. 2015 Synthesis of a new highly sensitive near-infrared fluorescent iridium(III) probe and its application for the highly selective detection of glutathione. *RSC Adv.* **5**, 85 095–85 104. (doi:10.1039/C5RA14847B)
55. Qu XY, Liu Q, Ji XN, Che HC, Zhou ZK, Shen Z. 2012 Enhancing the Stokes' shift of BODIPY dyes via through-bond energy transfer and its application for Fe^{3+}-detection in live cell imaging. *Chem. Commun.* **48**, 4600–4602. (doi:10.1039/c2cc31011b)
56. Qu XY, Li CJ, Chen HC, Mack J, Guo Z, Shen Z. 2013 A red fluorescent turn-on probe for hydrogen sulfide and its application in living cells. *Chem. Commun.* **49**, 7510–7512. (doi:10.1039/c3cc44128h)